

Structural insights for the design of new PPAR γ partial agonists with high binding affinity and low transactivation activity

Laura Guasch · Esther Sala · Cristina Valls ·
Mayte Blay · Miquel Mulero · Lluís Arola ·
Gerard Pujadas · Santiago Garcia-Vallvé

Received: 18 March 2011 / Accepted: 10 June 2011 / Published online: 21 June 2011
© Springer Science+Business Media B.V. 2011

Abstract Peroxisome Proliferator-Activated Receptor γ (PPAR γ) full agonists are molecules with powerful insulin-sensitizing action that are used as antidiabetic drugs. Unfortunately, these compounds also present various side effects. Recent results suggest that effective PPAR γ agonists should show a low transactivation activity but a high binding affinity to inhibit phosphorylation at Ser273. We use several structure activity relationship studies of synthetic PPAR γ agonists to explore the different binding features of full and partial PPAR γ agonists with the aim of differentiating the features needed for binding and those needed for the transactivation activity of PPAR γ . Our results suggest that effective partial agonists should have a hydrophobic moiety and an acceptor site with an appropriate conformation to interact with arm II and establish a hydrogen bond with Ser342 or an equivalent residue at arm III. Despite the fact that interactions with arm I increase the binding affinity, this region should be avoided in order to not increase the transactivation activity of potential PPAR γ partial agonists.

Keywords PPAR γ · Antidiabetics · PPAR γ partial agonists · Drug design · 3D-QSAR

Abbreviations

LBD Ligand binding domain
PPAR Peroxisome proliferator-activated receptor
QSAR Quantitative structure–activity relationship
SAR Structure activity relationship
TZDs Thiazolidinediones

Introduction

Peroxisome Proliferator-Activated Receptor γ (PPAR γ) is a ligand-activated transcription factor and a member of the nuclear receptor superfamily that plays an important role in adipogenesis and glucose homeostasis [1]. PPAR γ is activated by polyunsaturated fatty acids and their metabolites. This transcription factor regulates the expression of adipocyte-specific genes [2]; its function is, therefore, essential to fat cell formation, and PPAR γ full agonists stimulate triglyceride storage and the differentiation of preadipocytes into adipocytes [1]. Some PPAR γ full agonists, such as thiazolidinediones (TZDs), also have a powerful insulin-sensitizing action and are used as antidiabetic drugs [3]. Unfortunately, TZDs present various side effects, including weight gain, increased adipogenesis, renal fluid retention, bone fracture and increased incidence of cardiovascular events [4–6]. Other compounds with poor agonist activities for PPAR γ , called PPAR γ modulators or PPAR γ partial agonists, retain very good antidiabetic effects without these undesired side effects [4]. Therefore, several partial agonists of PPAR γ are being developed as new-antidiabetic drugs [6–8]. Analyses of a large number of crystallographic structures of the PPAR γ ligand-binding domain (LBD)

Electronic supplementary material The online version of this article (doi:10.1007/s10822-011-9446-9) contains supplementary material, which is available to authorized users.

L. Guasch · E. Sala · C. Valls · M. Blay · M. Mulero ·
L. Arola · G. Pujadas · S. Garcia-Vallvé (✉)
Grup de Recerca en Nutrigenòmica, Departament de Bioquímica
i Biotecnologia, Universitat Rovira i Virgili, Campus de
Sescelades, C/Marcel·lí Domingo s/n, 43007 Tarragona,
Catalonia, Spain
e-mail: santi.garcia-vallve@urv.net

L. Arola · G. Pujadas · S. Garcia-Vallvé
CTNS, Centre Tecnològic de Nutrició i Salut, Reus, Catalonia,
Spain

bound to an agonist have revealed that PPAR γ has at least two binding modes in a single binding site. These two binding modes correspond to full and partial agonists [9]. The binding pocket of PPAR γ has a Y-shaped form, consisting of an entrance (arm III) that branches off into two pockets. Arm I is extended toward H12, and arm II is situated between helix H3 and a β -sheet [10]. Arm I is the only substantially polar cavity of the PPAR γ ligand-binding domain, whereas arms II and III are mainly hydrophobic [10]. Full agonists occupy arm I, making a net of hydrogen bonds with the side chains of Ser289, His323, His449 and Tyr473 [9, 11]. These interactions stabilize H12 and are responsible for the transactivation activity of PPAR γ [9, 11]. In addition, full agonists also occupy arm II through a hydrophobic tail that is present in all ligands of this class [9, 11]. However, partial agonists interact mainly with arm III through a hydrogen bond with Ser342, but also with arm II through several hydrophobic interactions [12, 13]. This binding mode causes a lesser degree of H12 stabilization and an increase in the stabilization of H3 that affects the recruitment of coactivators and decreases the transactivation activity of PPAR γ [7, 14].

However, the previous model does not explain why compounds with different PPAR γ transactivation activities show the same insulin-sensitizing power. Recently, Choi et al. [15] revealed a new mechanism of action for the antidiabetic effect of some PPAR γ agonists. This mechanism is completely independent of the classical PPAR γ transactivation activity and relies instead on inhibition of the phosphorylation of PPAR γ at Ser273, thereby preventing the unregulated expression of some genes, including adiponectin (a fat-cell-selective gene, the expression of which is altered in obesity) and adiponectin (an insulin-sensitizing adipokine) [15]. This alternative mechanism could clarify a long-standing paradox of why PPAR γ activation by a wide range of ligands does not always correlate with the ligands' in vivo efficacy [16]. With this new knowledge, many research groups have had to accordingly shift their focus from their past drug discovery efforts on PPAR γ , which were focused exclusively on potency and agonist activity. It is now necessary to develop effective and safe antidiabetic therapies that maximize the inhibition of PPAR γ phosphorylation at Ser273 and reduce the side effects observed with current PPAR γ drugs [8, 15]. It seems likely that at least some of the problematic side effects of PPAR γ full agonists, such as weight gain or fluid retention, may occur through classical agonist action and that a substantial portion of the therapeutic benefits of full and partial PPAR γ agonists occurs through the inhibition of the PPAR γ phosphorylation at Ser273 [15]. Thus, an effective partial agonist of PPAR γ would have a weak transactivation activity and high phosphorylation inhibitory activity on PPAR γ at Ser273. This kind of compound would maintain its antidiabetic effects

while reducing undesired side effects. Until researchers shift their focus to study the potency of the phosphorylation inhibitory activity at Ser273, binding affinity would be used instead to evaluate potential drug candidates. In this sense, the antidiabetic potency of PPAR γ ligand drugs correlates very well with their binding affinities [17]. In the present study, after reviewing the binding features of full and partial agonists, we use several structure activity relationship (SAR) studies of synthetic PPAR γ agonists to explore the different binding features of full and partial PPAR γ agonists. Our goal was to differentiate the features needed for binding from those needed for the transactivation activity of PPAR γ . Thus, our rationale consists of defining which interactions between the ligand-binding domain of PPAR γ and its ligands increase the binding affinity without increasing the PPAR γ transactivation activity. This information would allow us to predict the features that will produce optimal PPAR γ agonists for use as antidiabetic drugs.

Computational methods

Datasets

A dataset of 205 PPAR γ agonists with measured IC₅₀ values (*i.e.*, binding affinity measured by the displacement of a radiolabeled full agonist) and transactivation activity was assembled from several SAR studies [18–29] (see Table 1). The IC₅₀ (nM) values were then transformed to $-\log$ IC₅₀ (pIC₅₀) (see Supporting Information Table S1). The transactivation activities were expressed as the percentage of maximal activation relative to the full agonist rosiglitazone (% max activation) (see Supporting Information Table S2). All compounds were drawn with ChemDraw Ultra v11.0 (CambridgeSoft Corporation, Cambridge, MA, USA; <http://www.cambridgesoft.com>), and their 3D structures were minimized with the LigPrep v2.4 program (Schrödinger LLC., Portland, USA; <http://www.schrodinger.com>) using an OPLS_2005 force field at pH 7.0 with the rest of the parameters at default.

Clustering

A structural similarity analysis of all PPAR γ agonists was performed using the Canvas v1.2 program (Schrödinger LLC., Portland, USA; <http://www.schrodinger.com>). For each compound, a set of MOLPRINT2D fingerprints was calculated using the default parameters. A similarity matrix, based on the Tanimoto similarities between each set of fingerprints, was calculated. In order to classify the compounds into several clusters, a Tanimoto cutoff of 0.8

Table 1 Structure activity relationship (SAR) studies of the PPAR γ agonists used in the current study

Series	Cluster	Transactivation activity (% max. activation) ^a		Binding affinity pIC ₅₀		Ref
		No. ligands	Activity range	No. ligands	Activity range	
<i>sar1</i>	1	18	4–33	30	6.50–8.70	[18]
<i>sar2</i>	2	11	20–51	13	7.77–9.00	[19]
<i>sar3</i>	2	13	21–97	17	5.20–9.00	[20]
<i>sar4</i>	2	8	19–33	11	6.96–9.00	[21]
<i>sar5</i>	2	18	14–47	19	6.14–9.00	[22]
<i>sar6</i>	3	–	–	16	5.44–7.00	[23]
<i>sar7</i>	1	–	–	30	5.03–9.00	[24]
<i>sar8</i>	4	12	26–65	11	4.91–8.10	[25]
<i>sar9</i>	4	9	24–71	–	–	[26]
<i>sar10</i>	4	10	30–92	–	–	[27]
<i>sar11</i>	3	20	25–89	–	–	[28]
<i>sar12</i>	5	17	19–93	–	–	[29]

^a % of maximal activation relative to the full agonist rosiglitazone

was used. Seven groups of compounds were then obtained. Some of the groups were grouped together because the compounds they contained were chemically very similar, i.e. they contained the same core scaffold, obtaining at the end five different clusters of compounds. The compounds of each cluster represent therefore a group of very similar compounds, with an average Tanimoto coefficient of their MOLPRINT2D fingerprints greater than 0.8. The similarity matrix was also used as an input for the DendroUPGMA server (<http://genomes.urv.es/UPGMA/>) [30] to represent, as a dendrogram, the chemical similarities between molecules.

Pharmacophore construction

Energetically optimized, structure-based pharmacophores were constructed with the Glide v5.6 program (Schrödinger LLC., Portland, USA; <http://www.schrodinger.com>). This program accurately characterizes protein–ligand interactions based on energetic contributions such that energetically favorable features are incorporated into the pharmacophore [31]. The Glide XP scoring function was used to obtain an energetic description of each complex. The pharmacophore sites are ranked based on the Glide XP energies, and the most favorable sites are selected for the pharmacophore hypothesis. Aromatic rings were considered as hydrophobic groups. The PPAR γ residues that interact with the sites of the above pharmacophores were visualized with the LigandScout v2.03 program (Inte:ligand, Vienna, Austria, <http://www.inteligand.com/ligandscout/>) [32].

Molecular alignments

The most crucial step for a 3D-QSAR construction model is the alignment of the molecules. We chose a structure-based docking strategy that was carried out using the poses predicted by docking using the Glide v5.6 program (Schrödinger LLC., Portland, USA; <http://www.schrodinger.com>). We only analyzed compounds with a similar chemical structure that we predicted that have very similar binding features to the receptor. These compounds were docked within the binding site of the 2Q5P PDB structure. The binding site was defined using the Receptor Grid Generation panel with the default options. Standard-precision (SP) docking was selected for screening the ligands. We selected the flexible docking mode, meaning that Glide internally generated conformations during the docking process. We did not request any constraints for docking. Each docking run recorded at most twenty poses per ligand that survived the post-docking minimization. GlideScore was used as the fitness function. The best scoring pose was selected for each ligand and used as an input structure for subsequent 3D-QSAR analyses. Moreover, to confirm that the docked poses that we obtained were realistic, we inspected manually the group of best scoring poses for each compound of the selected clusters to confirm that they contain the important intermolecular interactions with the receptor that we detect at the binding features analysis (and that, obviously, are also present in the 2Q5P complex). In addition, a cross docking analysis of the molecules used to build the 3D-QSAR with other PPAR γ conformations derived from PDB complexes (i.e., 2Q5S and 2P4Y) showed similar results to the ones obtained with 2Q5P. Thus, this knowledge-based selection of docked poses ensures their realism.

Generation of the 3D-QSAR models

The selected conformations of the ligands, obtained with the previously described alignment protocol, were used for the generation of a pair of 3D-QSAR models (one for pIC₅₀ and another for the percentage of maximal activation). The Phase v3.2 program (Schrödinger LLC., Portland, USA; <http://www.schrodinger.com>) was employed to carry out the calculations using the Atom-Based 3D-QSAR panel. In the atom-based 3D-QSAR, a molecule is treated as a set of overlapping van der Waals spheres. To encode the basic characteristics of the local chemical structure, each atom (and hence each sphere) is placed into one of six categories according to a simple set of rules: hydrogen atoms attached to polar atoms are classified as hydrogen bond donors (D); carbons, halogens, and C–H hydrogens are classified as hydrophobic/non-polar (H); atoms with an explicit negative ionic charge are classified as negative ionic (N); atoms with an explicit positive ionic charge are classified as positive ionic (P); non-ionic nitrogen and oxygen atoms are

classified as electron-withdrawing (W); and all other types of atoms are classified as miscellaneous (X) [33]. The docking-predicted conformations of each ligand were first imported into the program together with their activity data. Then, training and test sets were chosen randomly using the Phase program. We chose a high training set percentage (80%) because the main aim of our models was to explain the relation between the selected ligands and their activities, not to predict activity values. Furthermore, in order to discard a possible influence of the splitting of the ligands into the training and test subsets on the resulting pair of 3D-QSAR models, we (1) randomly selected other 10 different training/test sets, (2) obtained their corresponding pairs of 3D-QSAR models, and (3) check their similarity relative to the initial pair of models by visual inspection. The 3D-QSAR model partitions the space occupied by the ligands into a cubic grid. Any structural component can occupy part of one or more cubes. The size of the cubes selected was 1 Å. The independent variables in the regression were given by the binary-valued occupancies (“bits”) of the cubes (by structural components), while the dependent variables were the transactivation activity or the binding affinity. The regression was done by constructing a series of models with an increasing number of partial least square (PLS) factors. The accuracy of the models increases when the number of PLS factors increases until over-fitting starts to occur.

Statistical validations of the 3D-QSAR models

The performance of the initial pair of 3D-QSAR models was evaluated by measuring the accuracy of the predictions. The statistical parameters that were used to evaluate the predictions for the training set were: (a) the coefficient of determination (R^2); (b) the standard deviation of regression (SD); (c) the F statistic, which measures the overall significance of the model; (d) the statistical significance (P), which measures the probability that the correlation could occur by chance; and (e) a stability value, which has a maximum value of 1 and measures the stability of the model predictions with changes in the training set composition. The parameters used to evaluate the predictions for the test set were: (a) Q^2 , the equivalent of R^2 for the test set; (b) the root-mean-square error (RMSE); and (c) the Pearson correlation coefficient (r).

Results and discussion

Binding features of partial agonists

A total of 205 structures of PPAR γ agonists were retrieved from 12 SAR studies (*sar1-12*) of synthetic PPAR γ agonists

(Table 1) [18–29]. Based on their chemical similarities, these 205 compounds can be grouped into five clusters (Fig. 1). Cluster 1 is composed of ligands from *sar1* (aryl indole-2-carboxylic acids) and *sar7* (*N*-sulfonyl-2-indole carboxamides), which consist of an indole system that contains a carboxylic group or a sulfonyl group at the second position [18, 24]. In essence, all of the ligands from this cluster have two lipophilic parts on either side of an acidic center. Cluster 2 is the largest family and contains compounds from *sar2* (3-acylindole-1-benzylcarboxylic acids) [19], *sar3* (benzoyl 2-methyl indoles) [20], *sar4* (*N*-benzylindoles) [21] and *sar5* (7-azaindoles) [22]. Compounds from this cluster have an indole group, like the compounds from cluster 1, but otherwise follow a different pattern. These compounds are made up of an acidic head and a lipophilic tail. Cluster 3 contains a series of ligands from *sar6* (5-substituted 2-benzoylaminobenzoic acids) [23] and *sar11* (2,4,6-trisubstitutedpyrimidine-5-carboxylic acid derivatives) [28]. Although the *sar11* series seems to be more related to the *sar12* series shown in Fig. 1, the core scaffolds of the *sar11* and *sar6* series are chemically very similar. We therefore decided to cluster these two series together in cluster 3. The compounds from this cluster follow the same pattern as cluster 1, but without the presence of an indole group. The *sar8* [25], *sar9* [26] and *sar10* [27] series form cluster 4. The compounds from this cluster are derivatives of telmisartan, a compound that, in addition to being a PPAR γ partial agonist, is also a selective angiotensin II AT1 receptor blocker. Finally, cercosporamide derivatives from the *sar12* series [29] form cluster 5.

With the aim of analyzing the binding differences between different PPAR γ agonists, we constructed at least one energetically optimized pharmacophore [31] for each of the above clusters. This methodology quantifies the importance of each pharmacophore feature and allowed us to analyze the differences of receptor-ligand contacts between clusters. Table 2 shows the eight energy-based pharmacophores constructed from eight PDB structures that contain the PPAR γ LBD crystallized with a partial agonist. Most of the pharmacophore sites are aromatic rings, highlighting the importance of hydrophobic interactions for the binding of PPAR γ agonists with the receptor. Another significant feature is the presence of an acceptor site together with a negative site in the majority of the pharmacophores. This site corresponds to a carboxylic group present in the majority of the PPAR γ partial agonists that forms a hydrogen bond with the Ser342 from the LBD of PPAR γ . A comparison of the energy-based pharmacophores between clusters shows that the pharmacophores from clusters 1, 2 and 3 are similar, although the positions of the hydrophobic sites vary. The pharmacophores from clusters 4 and 5 are, however, slightly different. They contain an additional donor site, and the hydrophobic sites

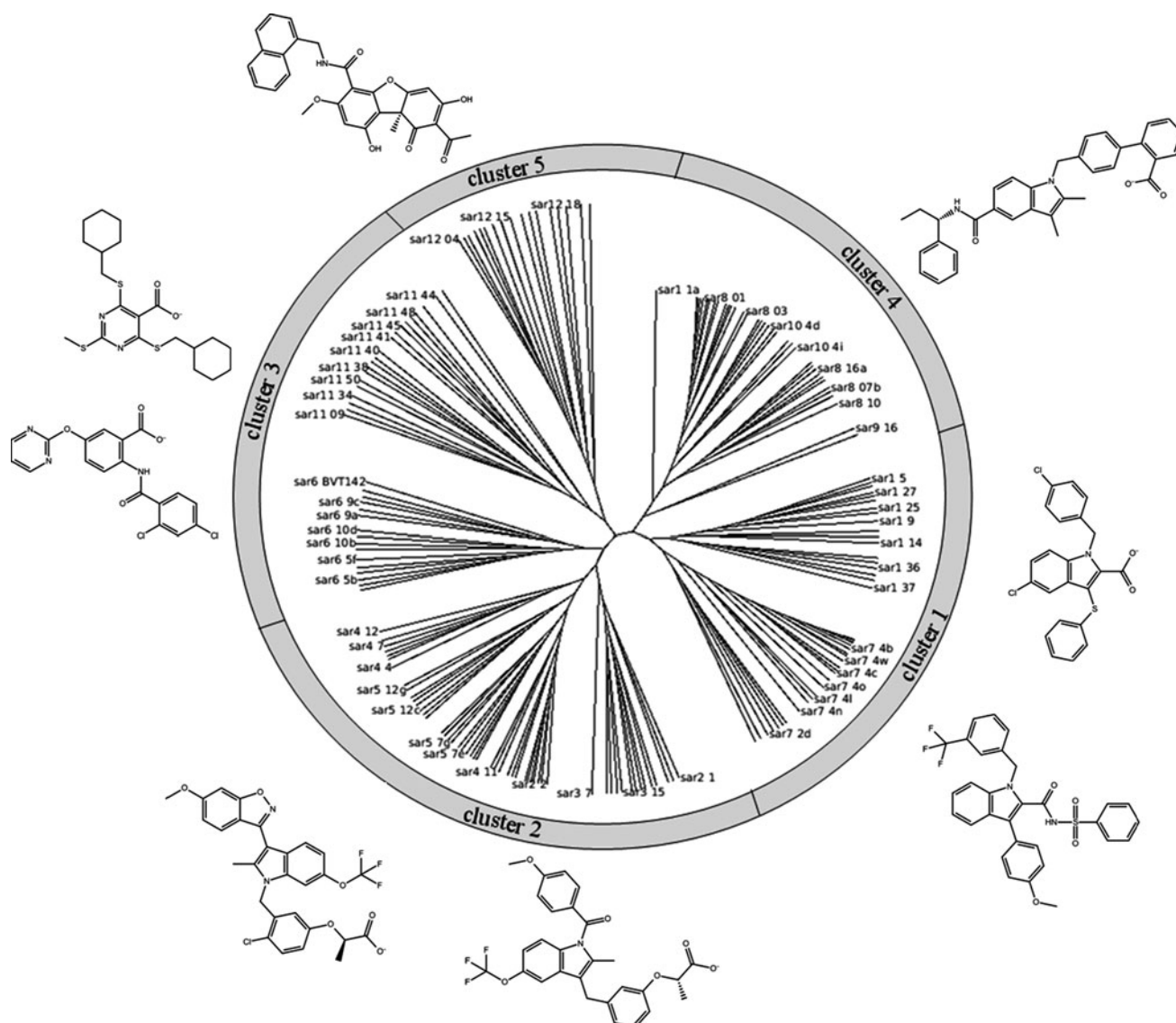


Fig. 1 Representation of PPAR γ partial agonist clusters. A total of 205 synthetic compounds from 12 SAR series were clustered by comparing their MOLPRINT2D fingerprints. The 2D structure of a representative member of each cluster is also shown

occupy a different region when compared with the pharmacophores from clusters 1, 2 and 3. Table 2 also shows the energy-based pharmacophore of a PPAR γ full agonist. This pharmacophore has sites similar to those of the previous pharmacophores, but their locations are very different, highlighting the binding differences between full and partial PPAR γ agonists.

Table 2 also shows the binding differences between full and partial agonists (and between some partial agonists) from the receptor point of view. In this table, the PPAR γ residues that interact with each site of the pharmacophores are shown. The hydrophobic interactions between Ile281, Ala292, Ile326, Ile341, Leu330, Leu333, Val339, Met348, Leu353 and Met364 and the hydrophobic sites of the ligands are conserved in the majority of the structures (see

Table 2), even for the full agonist. The residue that interacts through a hydrogen bond with the acceptor/negative site of the ligand differs depending on whether the ligand is a full or partial agonist. Partial agonists (with the exception of compounds from cluster 5) form a hydrogen bond with Ser342. However, the residues that interact through a hydrogen bond in full agonists are usually Ser289 and Tyr473. There are other binding differences between partial and full agonists. If we split the LBD of PPAR γ into three parts, arm I, arm II and arm III (see Fig. 2), we observe that the partial agonists (with the exception of compounds from cluster 4) basically interact with arms II and III, but the full agonists basically interact with arms I and II (see Table 2). Thus, in agreement with previous results [10], our analyses show that full and partial agonists

Table 2 Energy-based pharmacophores for eight structures that contain the PPAR γ ligand-binding domain crystallized with a partial agonist plus one structure complexed with a full agonist

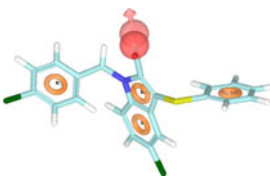
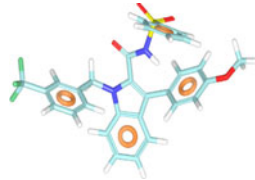
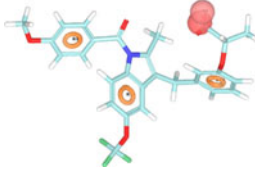
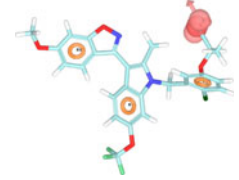
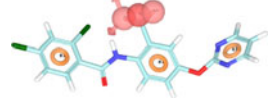
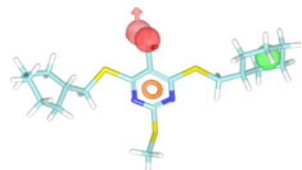

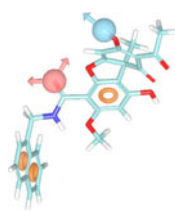
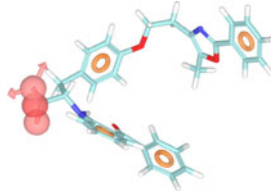
Cluster	PDB code	Energetic pharmacophore	Contact residues		
			ARM I	ARM II	ARM III
1	2Q5S		Ile326 Phe363	Ile249 Ile281 Val339 Ile341 Met348 Leu353 Met364	Ala292 Leu330 Ser342*
	2HFP		Ile326	Ile281 Met329 Val339 Ile341 Met348 Leu353 Met364	Ile262 Lys265* Arg288 Ala292 Leu330 Leu333 Ser342*
2	2Q5P		Ile326 Tyr327	Phe264 Ile281 Val339 Ile341 Met348	Arg288 Ala292 Leu330 Leu333 Ser342*
	2P4Y		Ile326 Tyr327 Phe363	Ile281 Met329 Val339 Ile341 Met348 Leu353 Met364	Phe287 Ala292 Leu330 Leu333 Ser342*
3	2Q6S		–	Ile249 Leu255 Phe264 Val339 Met364	Ala292 Leu330 Leu333 Ser342*
	Cmpd 50		Ile326	Leu255 Ile281 Val339 Ile341 Leu353 Met364	Ile262 Thr268 Ala292 Leu330 Leu333 Ser342*
4	3KMG		Phe282 Ser289* Ile326 Tyr327* Phe363 Leu453 Leu465 Leu469	Ile281 Val339 Ile341 Met348 Met364	Arg288* Ala292 Leu330 Leu333 Ser342*

Table 2 continued

Cluster	PDB code	Energetic pharmacophore	Contact residues		
			ARM I	ARM II	ARM III
5	3LMP		Ile326	Met334 Leu353 Met364	Leu330 Cys285*
Full agonist	1FM9		Phe282 Ser289* Ile326 Phe360 Phe363 Leu453 Ile456 Leu465 Leu469 Tyr473*	Ile281 Val339 Ile341 Met348 Leu353 Met364	Leu330

Pink spheres represent hydrogen bond acceptors, green spheres represent hydrophobic groups, orange rings represent aromatic rings, light-blue spheres represent hydrogen bond donors, and red spheres represent negative ionizable groups. The PPAR γ residues involved in the interaction with the ligand are also shown. All interactions correspond to hydrophobic interactions, with the exception of the residues marked with an asterisk, which form hydrogen bonds with the polar groups of the ligands. The interactions conserved in the majority of the structures that contain a PPAR γ agonist are shown in bold. All energetic pharmacophores are presented in the same relative orientation in order to allow for an easier comparison. Contact residues were defined using LigandScout

show different binding patterns for the LBD of PPAR γ . The binding patterns of different partial agonists are also slightly different. Ligands from cluster 4 occupy arm I, like full agonists, and also make two additional hydrogen bonds with Ser289 and Tyr327 (see Table 2). Ligands from cluster 5 make few contacts with the LBD of PPAR γ because they are surrounded by several water molecules. The binding profiles of compounds from clusters 1, 2 and 3 are similar (see Table 2).

Generation of 3D-QSAR models

We selected the *sar1*, *sar2*, *sar3*, *sar4* and *sar5* series of PPAR γ agonists for the construction of two 3D-QSAR models. 3D-QSAR techniques have efficiently provided models in reasonable agreement with those deduced by the crystal structure of PPAR γ complexes [34]. We used this methodology not for predicting the activity or binding affinity of putative PPAR γ agonists, but rather to analyze which interactions between the LBD of PPAR γ and its ligands increase the binding affinity without increasing the PPAR γ transactivation activity. The *sar1*, *sar2*, *sar3*, *sar4* and *sar5* series were selected because for these compounds we have a wide range of measured IC₅₀ (i.e., binding affinity measured by the displacement of a radiolabeled full

agonist) values, tested under the same assay conditions, and values for the transactivation activity (see Table 1). Ligands from *sar8* were not used because their binding mode is quite different from that used by the agonists from clusters 1 and 2 (see Table 2). The *sar1*, *sar2*, *sar3*, *sar4* and *sar5* series form clusters 1 and 2 in Fig. 1 and contain a set of 82 indole-based PPAR γ agonist derivatives with a similar binding profile. With these compounds, we constructed two atom-based 3D-QSAR models, one analyzing the binding affinity between the ligands and PPAR γ (called the pIC₅₀ model) and one analyzing the transactivation activity of PPAR γ (called the transactivation model). For the first model, we used values of pIC₅₀, and for the second, we used the percentage of maximal activation relative to the full agonist rosiglitazone. Activation levels that reach the maximal activation of rosiglitazone are considered full agonists, while those reaching 20–60% of rosiglitazone maximal activation are considered partial agonists. Table 3 and Fig. 3 show the statistic fits of the constructed 3D-QSAR models. For both models, as it is shown in Fig. 3, the activity values of the ligands from the training and test sets are homogeneously distributed along all the activity range. In both models, to avoid an over-fitting effect, two PLS factors were chosen. The Pearson correlation coefficient of the pIC₅₀ model was 0.77 with an R²

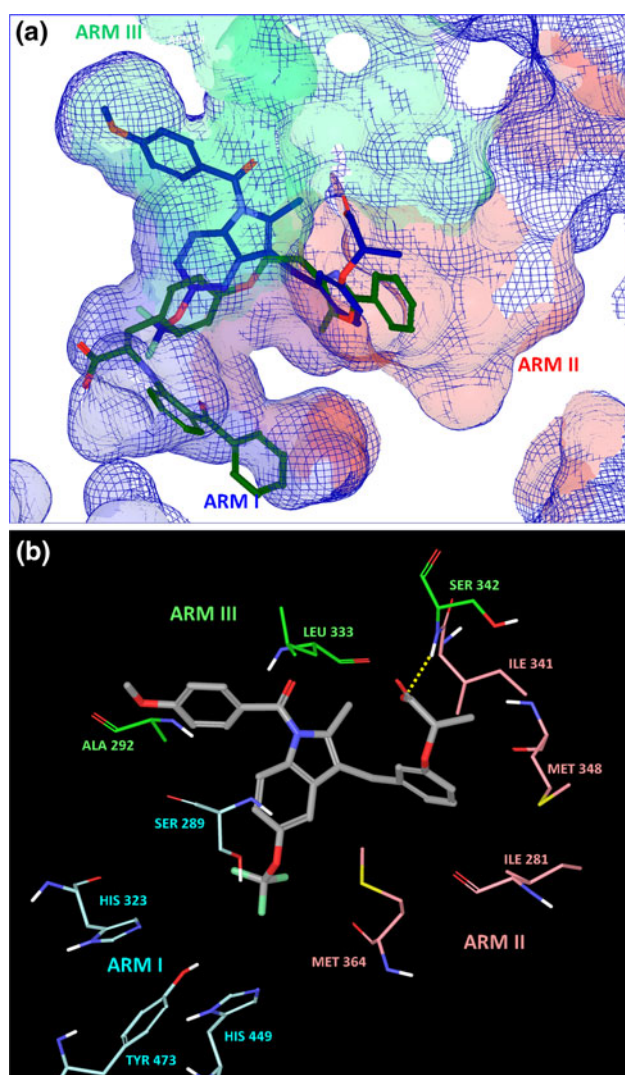


Fig. 2 **a** The ligand-binding domain (LBD) of PPAR γ complexed with a partial agonist, a benzoyl 2-methyl indole derivate (MRL-24 from PDB 2Q5P), colored in blue, superimposed with the structure of a full agonist, farglitazar, colored in green. The partial agonist occupies mainly arm II and arm III of the LBD of PPAR γ , but the full agonist occupies mainly arm I and arm II. **b** The main interactions between the PPAR γ partial agonist MRL-24 and the LBD of PPAR γ . The conserved hydrophobic interactions between Ile281, Ala292, Ile326, Ile341, Leu333, Met348 and Met364 and the hydrophobic sites of MRL-24 are shown. These interactions are common to nearly all PPAR γ agonists, including full agonists. Hydrogen bonds between Ser342 and the carboxylic acid from MRL-24 are also shown by a dashed yellow line. This hydrogen bond is conserved between some PPAR γ partial agonists but not for full agonists

for the training set and a Q^2 for the test set of 0.67 and 0.55, respectively. For the transactivation model, the Pearson correlation coefficient was 0.72 with an R^2 for the training set and a Q^2 for the test set of 0.71 and 0.40, respectively. The low Q^2 values imply that there is a greater difference between the experimental values of binding affinity and transactivation activity and the values predicted by each

model. This difference is more important when predicting the transactivation activity of full agonists (see Fig. 3b). This may be due to the fact that the great majority of compounds in the dataset used are partial agonists. The R^2 values for the training set are better. As our main purpose was to use the 3D-QSAR models for analyzing the interactions between the LBD of PPAR γ and a group of similar PPAR γ agonists, the R^2 values are more relevant. These R^2 values and the scatter plots for the training set in Fig. 3 indicate a reasonably good correlation between the predicted and experimental activities and validate the use of both models.

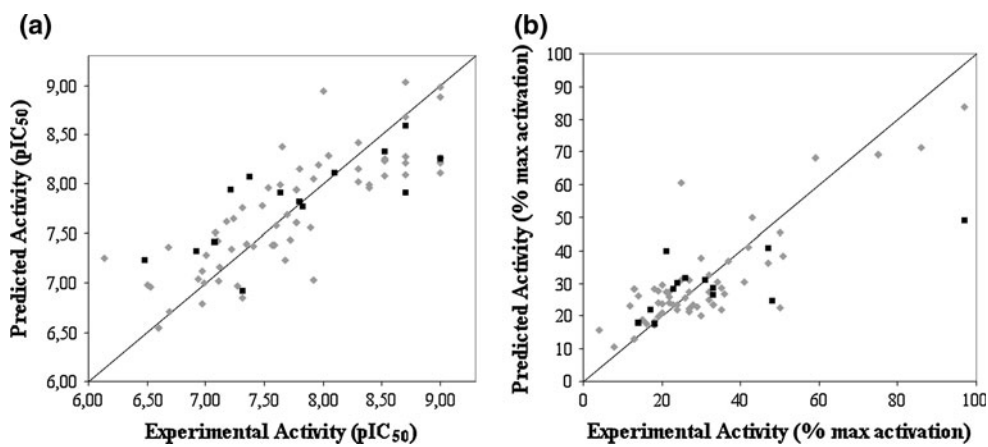
Figures 4 and 5 show the representation of the 3D-QSAR models. In these figures, the cubes that represent the model are displayed and colored according to the sign of their coefficient values. Blue and red cubes are used, respectively, for positive and negative coefficients and indicate regions that increase or decrease the analyzed parameter. One of the advantages of using these representations is that the position of the cubes of the 3D-QSAR model can be compared with the positions of the amino acid residues in the active site. This might give an insight as to which functional groups are desirable or undesirable at certain positions in a molecule. Figure 4b shows the favorable and unfavorable regions for the binding affinity. Similar favorable and unfavorable regions were obtained when ten additional 3D-QSAR models were generated using different training set selections obtained at random (results not shown). The favorable regions for binding are located at regions that interact with arms I and II and the right part of arm III (which includes Ser342) of the LBD of PPAR γ . When viewing the 3D-QSAR model by atom type, we see that the hydrophobic (Fig. 4c) and the electron-withdrawing contributions (Fig. 4d) are the most important for the binding affinity of the compounds analyzed (whereas the rest of the contributions have a very limited role in binding affinity; results not shown). The electron-withdrawing contributions are favorable at arm I, where hydrogen bonds with Ser289, His323, His449 and Tyr473 can be established, and arm II, where a hydrogen bond with Ser342 is common to most PPAR γ partial agonists. Hydrophobic interactions are the most important binding forces between PPAR γ agonists and the LBD of PPAR γ . The representation of the 3D-QSAR model in Fig. 4c suggests that, when more hydrophobic interactions occur with arm I and arm II of the LBD of PPAR γ , a greater binding affinity is seen in the compound. Figure 4e and f display the cubes of the 3D-QSAR model grid that are occupied by two compounds from the SAR series analyzed. In these representations, we can see which parts of the ligand have a positive or a negative contribution to the parameter analyzed, which is, in this case, the binding affinity. Figure 4e shows the *sar1_24* compound [18],

Table 3 Statistics of the best 3D-QSAR models for analyzing the binding affinity (pIC₅₀ model) and the transactivation activity of PPAR γ (% max activation model) derived from an 80% randomly selected training set

Model	# Factors	SD	R ²	F	P	Stability	RMSE	Q ²	Pearson-r
pIC ₅₀	1	0.62	0.31	26.1	3.8e-06	0.94	0.68	0.14	0.43
	2	0.43	0.67	58.5	1.53e-14	0.49	0.49	0.55	0.77
	3	0.36	0.78	64.5	3.66e-18	0.38	0.57	0.40	0.63
	4	0.24	0.90	121.8	1.2e-26	0.15	0.63	0.26	0.51
	5	0.19	0.94	166.7	1.55e-31	-0.02	0.63	0.25	0.50
% max activation	1	13.64	0.42	38.2	9.36e-08	0.85	17.83	0.28	0.55
	2	9.69	0.71	64.4	8.57e-15	0.55	16.27	0.40	0.72
	3	6.4	0.88	121.1	3.42e-23	0.29	17.61	0.30	0.63
	4	4.75	0.93	175.7	8.78e-29	0.22	17.31	0.32	0.64
	5	2.98	0.97	372.3	9.95e-38	0.15	16.33	0.40	0.72

See the “[Computational methods](#)” section for the meaning of the statistical parameters used. To avoid an over-fitting effect, two factor models (showed in bold) were chosen

Fig. 3 Scatter plots for the two factors **a** pIC₅₀ and **b** percentage of maximal activation models applied to the training set (colored in gray) and the test set (colored in black)

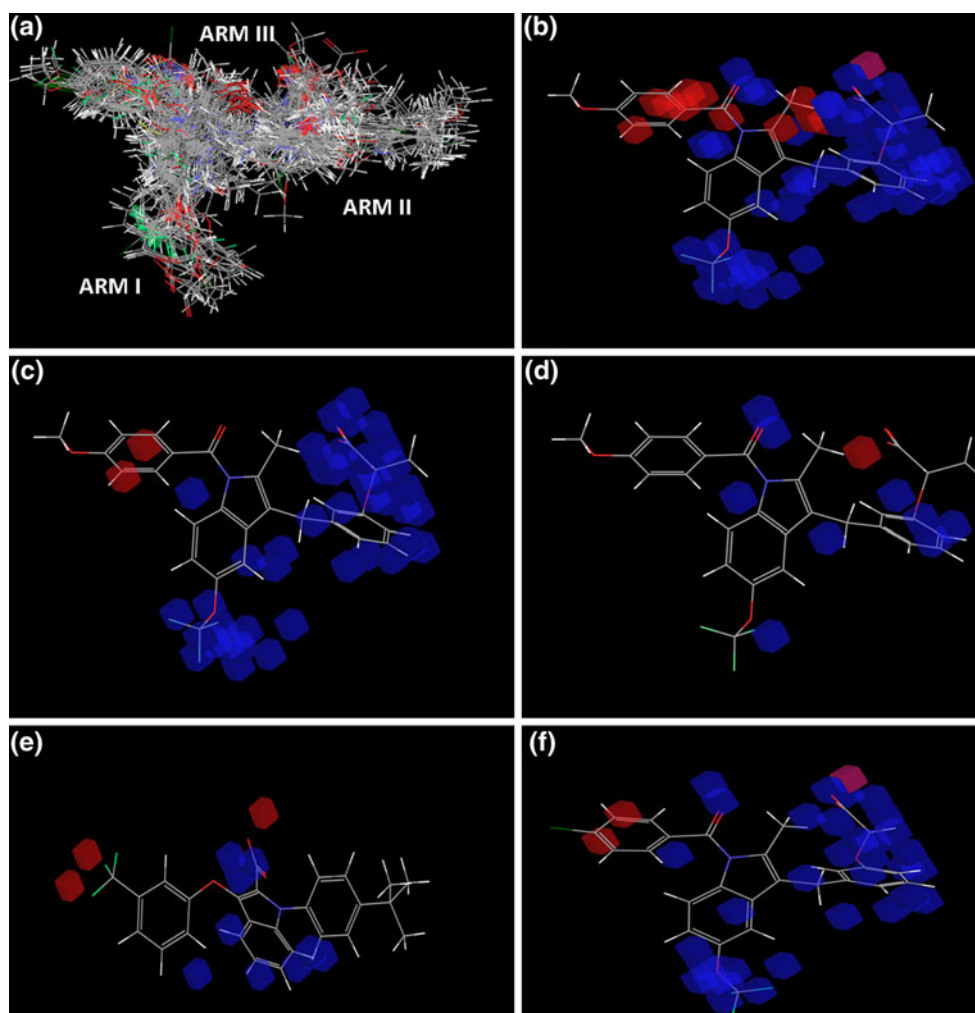


which has one of the lowest binding affinities in this series. Our 3D-QSAR model explains the low binding affinity of this compound because, although it can partially interact with arm II through a carboxylic group (see the upper blue cubes in Fig. 4e), it lacks a hydrophobic moiety at indole position 6 to interact with arm I. This compound also contains a trifluoromethyl group, a group with high electronegativity, located in the hydrophobic environment of arm III (see the red cubes in Fig. 4e). When the compound from our ligand dataset with the highest binding affinity (i.e., *sar2_1* in Fig. 4f) is considered in the context of the model, we see an excellent fit with the blue areas of the model (see Fig. 4f).

Figure 5 shows a representation of the transactivation model. In this model, the transactivation activity of PPAR γ is the variable analyzed. Figure 5a shows the favorable and unfavorable regions for transactivation activity. Similar favorable and unfavorable regions were obtained when ten additional 3D-QSAR models were generated using different training set selections obtained at random (results not shown). The favorable regions are located at arm I and at part of arm III. Interestingly, unfavorable regions are located at arm II and the right part (which corresponds to Ser342) of arm III. Figure 5b–d show that the main

contribution to the transactivation activity of PPAR γ is caused by hydrophobic interactions, specifically the hydrophobic interactions that can be established with the hydrophobic residues of the LBD of PPAR γ that form arm II and part of arm I (see Fig. 5b). Hydrophobic interactions with arm II and part of arm III are marked as unfavorable in the model (Fig. 5b). This effect is due to the fact that partial agonists do not occupy arm I but do occupy arm II and the right part of arm III. In addition, an unfavorable hydrophobic interaction is also localized at arm I (see the red cubes at the bottom and left side of Fig. 5b). A carboxylic group that makes a hydrogen bond with Ser289 may occupy this part of the ligand, especially for full PPAR γ agonists. This interaction is crucial for the stabilization of H12 and for the transactivation activity of PPAR γ . Thus, when this region is occupied by a hydrophobic group, a hydrogen bond cannot be established, and the transactivation activity of PPAR γ decreases. The importance of this interaction for the transactivation activity of PPAR γ is also visualized in Fig. 5c and d, when the electron-withdrawing and negatively charged contributions are represented in the transactivation model. In both figures, a blue cube at arm I (at the bottom of the figures) represents the importance of polar interactions in

Fig. 4 Representation of the pIC50 model. The structural alignment of the selected docking poses of all compounds **a** was used to construct an atom-based 3D-QSAR model. *Blue* and *red cubes* indicate, respectively, regions that are favorable and unfavorable for binding to the LBD of PPAR γ . The thresholds used for considering a region with a positive or negative contribution were 1.0×10^{-2} and -1.4×10^{-2} , respectively. The complete 3D-QSAR model is displayed in panel **b**, whereas panels **c** and **d** show the hydrophobic and electron-withdrawing contributions, respectively. Panels **e** and **f** show the cubic volume elements that are occupied by one of the compounds of the series with the lowest (i.e., sar1_24) and the highest (i.e., sar2_1) binding affinity, respectively. All panels are presented in the same relative orientation in order to allow for an easier comparison

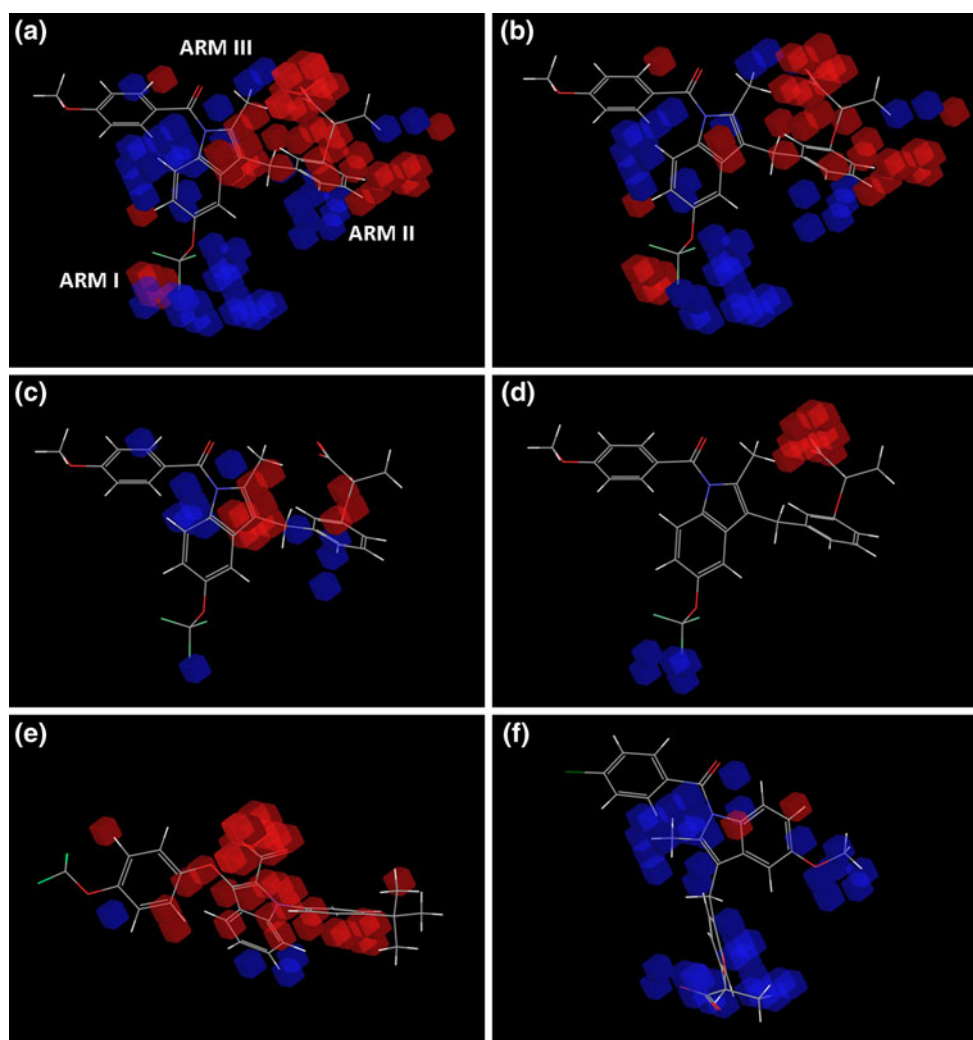


this region. Figure 5d also shows that the negatively charged contributions at the right part of arm III are unfavorable for the transactivation activity. This negative contribution reflects the fact that most partial agonists have a carboxylic group at this region that forms a hydrogen bond with Ser342. This hydrogen bond neither stabilizes H12 nor activates the transactivation activity of PPAR γ . As the majority of partial agonists form this hydrogen bond and their transactivation activity is low, the model marks this interaction as unfavorable for the transactivation activity. Figure 5e and f show, respectively, the 3D-QSAR model represented only by the cubic volume elements that are occupied by one of the most inactive compounds (i.e., the *sar1_6* compound) and the most active compound (i.e., the *sar3_12* compound) in terms of transactivation activity. The *sar1_6* compound [18] has only a maximal transactivation activity of 8% relative to rosiglitazone. Figure 5e shows that this ligand basically occupies arm III and arm II of the receptor and makes hardly any of the favorable interactions shown as blue cubes in Fig. 5. The *sar3_12* compound [20] has a maximal transactivation activity of

97% relative to rosiglitazone. This compound fits the blue areas of the 3D-QSAR model perfectly, as it can interact with the receptor through the favorable regions at arms I, II and III (see Fig. 5f).

Arm I of the LBD of PPAR γ is an important part for the binding and the transactivation activity of PPAR γ ligands. The ligands that occupy this arm interact with PPAR γ through a series of hydrophobic interactions and a net of hydrogen bonds with the side chains of Ser289, His323, His449 and Tyr473. These interactions stabilize H12 and are responsible for the transactivation activity of PPAR γ [9, 11]. When a hydrophobic group occupies the region of the carboxyl group responsible for the net of hydrogen bonds with the side chains of Ser289, His323, His449 and Tyr473, the transactivation activity of PPAR γ decreases (see Fig. 5). Other regions of the LBD of PPAR γ that also contribute to the transactivation activity of PPAR γ include the regions of arms III and II that are closer to arm I. Hydrophobic interactions in these regions are favorable for the transactivation activity of PPAR γ (see Fig. 5). However, the region of arm III furthest from arm II does not

Fig. 5 Representation of the % of maximal transactivation model. *Blue* and *red cubes* indicate, respectively, regions that are favorable and unfavorable for the transactivation activity of PPAR γ . The thresholds used for considering a region with a positive or negative contribution were 2.0×10^{-1} and -2.0×10^{-1} , respectively. The complete 3D-QSAR model is displayed in panel **a**, whereas panels **b**, **c** and **d** show the hydrophobic, electron-withdrawing and negatively charged contributions, respectively. Panels **e** and **f** show, respectively, the cubic volume elements that are occupied by one of the least actives (i.e., sar1_6) and one of the most actives (i.e., sar3_12) compounds. All panels are presented in the same relative orientation in order to allow for an easier comparison



contribute to this activity. This region, which includes Ser342, is the region most occupied by partial agonists. Hydrophobic interactions between the PPAR γ residues from arms I and II and the hydrophobic groups of PPAR γ ligands are very important for their binding (see Fig. 4). In addition, partial agonists can establish a hydrogen bond with Ser342. Because arm I contributes significantly to the transactivation activity of PPAR γ , this region must not be occupied by potential PPAR γ partial agonists.

Conclusion

The ideal PPAR γ partial agonists to be used as antidiabetic compounds should show a low transactivation activity but a high binding affinity to inhibit phosphorylation at Ser273. Our models suggest that effective partial agonists should have a hydrophobic moiety and an acceptor site with an appropriate conformation to interact with arm II and to establish a hydrogen bond with Ser342 or an equivalent

residue. Despite the fact that interactions with arm I increase the binding affinity, this region should be avoided in order to decrease the transactivation activity of potential PPAR γ partial agonists.

Acknowledgments This manuscript was edited for English language fluency by American Journal Experts. This study was supported by Grant Number AGL2008-00387/ALI from the Ministerio de Educación y Ciencia of the Spanish Government and the ACCIÓ (TECCT10-1-0008) program (Generalitat de Catalunya). The authors wish to thank the Servei de Disseny de Fàrmacs (Drug Design Service) of the Catalonia Supercomputer Center (CESCA) for providing access to Schrödinger software.

References

- Berger J, Moller DE (2002) *Annu Rev Med* 53:409
- Willson TM, Lambert MH, Kliewer SA (2001) *Annu Rev Biochem* 70:341
- Lehmann JM, Moore LB, Smith-Oliver TA, Wilkison WO, Willson TM, Kliewer SA (1995) *J Biol Chem* 270:12953

4. Feldman PL, Lambert MH, Henke BR (2008) *Curr Top Med Chem* 8:728
5. Pourcet B, Fruchart J, Staels B, Glineur C (2006) *Expert Opin Emerg Drugs* 11:379
6. Jones D (2010) *Nat Rev Drug Discov* 9:668
7. Gelman L, Feige JN, Desvergne B (2007) *Biochim Biophys Acta* 1771:1094
8. Grether U, Klaus W, Kuhn B, Maerki HP, Mohr P, Wright MB (2010) *ChemMedChem* 5:1973
9. Farce A, Renault N, Chavatte P (2009) *Curr Med Chem* 16:1768
10. Zoete V, Grosdidier A, Michielin O (2007) *Biochim Biophys Acta* 1771:915
11. Pochetti G, Godio C, Mitro N, Caruso D, Galmozzi A, Scurati S, Liodice F, Fracchiolla G, Tortorella P, Laghezza A, Lavecchia A, Novellino E, Mazza F, Crestani M (2007) *J Biol Chem* 282:17314
12. Bruning JB, Chalmers MJ, Prasad S, Busby SA, Kamenecka TM, He Y, Nettles KW, Griffin PR (2007) *Structure* 15:1258
13. Montanari R, Saccoccia F, Scotti E, Crestani M, Godio C, Gilardi F, Liodice F, Fracchiolla G, Laghezza A, Tortorella P, Lavecchia A, Novellino E, Mazza F, Aschi M, Pochetti G (2008) *J Med Chem* 51:7768
14. Lu I, Huang C, Peng Y, Lin Y, Hsieh H, Chen C, Lien T, Lee H, Mahindroo N, Prakash E, Yueh A, Chen H, Goparaju CMV, Chen X, Liao C, Chao Y, Hsu JT, Wu S (2006) *J Med Chem* 49:2703
15. Choi JH, Banks AS, Estall JL, Kajimura S, Boström P, Laznik D, Ruas JL, Chalmers MJ, Kamenecka TM, Blüher M, Griffin PR, Spiegelman BM (2010) *Nature* 466:451
16. Houtkooper RH, Auwerx J (2010) *Nature* 466:443
17. Willson TM, Cobb JE, Cowan DJ, Wiethe RW, Correa ID, Prakash SR, Beck KD, Moore LB, Kliewer SA, Lehmann JM (1996) *J Med Chem* 39:665
18. Dropinski JF, Akiyama T, Einstein M, Habulihaz B, Doebber T, Berger JP, Meinke PT, Shi GQ (2005) *Bioorg Med Chem Lett* 15:5035
19. Liu W, Liu K, Wood HB, McCann ME, Doebber TW, Chang CH, Akiyama TE, Einstein M, Berger JP, Meinke PT (2009) *J Med Chem* 52:4443
20. Acton JJ, Black RM, Jones AB, Moller DE, Colwell L, Doebber TW, MacNaul KL, Berger J, Wood HB (2005) *Bioorg Med Chem Lett* 15:357
21. Liu K, Black RM, Acton JJ, Mosley R, Debenham S, Abola R, Yang M, Tschirret-Guth R, Colwell L, Liu C, Wu M, Wang CF, MacNaul KL, McCann ME, Moller DE, Berger JP, Meinke PT, Jones AB, Wood HB (2005) *Bioorg Med Chem Lett* 15:2437
22. Debenham SD, Chan A, Lau FW, Liu W, Wood HB, Lemme K, Colwell L, Habulihaz B, Akiyama TE, Einstein M, Doebber TW, Sharma N, Wang CF, Wu M, Berger JP, Meinke PT (2008) *Bioorg Med Chem Lett* 18:4798
23. Thor M, Beierlein K, Dykes G, Gustavsson AL, Heidrich J, Jendeberg L, Lindqvist B, Pegurier C, Roussel P, Slater M, Svensson S, Sydow-Bäckman M, Thornström U, Uppenberg J (2002) *Bioorg Med Chem Lett* 12:3565
24. Hopkins CR, O'neil SV, Laufersweiler MC, Wang Y, Pokross M, Meikel M, Evdokimov A, Walter R, Kontoyianni M, Petrey ME, Sabatakos G, Roesgen JT, Richardson E, Demuth TP (2006) *Bioorg Med Chem Lett* 16:5659
25. Lamotte Y, Martres P, Faucher N, Laroze A, Grillot D, Ancellin N, Saintillan Y, Beneton V, Gampe RT (2010) *Bioorg Med Chem Lett* 20:1399
26. Goebel M, Clemenz M, Staels B, Unger T, Kintscher U, Gust R (2009) *ChemMedChem* 4:445
27. Goebel M, Staels B, Unger T, Kintscher U, Gust R (2009) *ChemMedChem* 4:1136
28. Seto S, Okada K, Kiyota K, Isogai S, Iwago M, Shinozaki T, Kitamura Y, Kohno Y, Murakami K (2010) *J Med Chem* 53:5012
29. Furukawa A, Arita T, Satoh S, Wakabayashi K, Hayashi S, Matsui Y, Araki K, Kuroha M, Ohsumi J (2010) *Bioorg Med Chem Lett* 20:2095
30. Garcia-Vallvé S, Palau J, Romeu A (1999) *Mol Biol Evol* 16:1125
31. Salam NK, Nuti R, Sherman W (2009) *J Chem Inf Model* 49:2356
32. Wolber G, Langer T (2005) *J Chem Inf Model* 45:160
33. Dixon SL, Smondyrev AM, Knoll EH, Rao SN, Shaw DE, Friesner RA (2006) *J Comput Aided Mol Des* 20:647
34. Giaginis C, Theocharis S, Tsantili-Kakoulidou A (2009) *Mini Rev Med Chem* 9:1075